

徐建业, 王富芳, 梁汉东, 等. 北宋定窑茶叶末釉的微观结构与矿物形态学研究[J]. 岩矿测试, 2025, 44(1): 115-126. DOI: 10.15898/j.ykcs.202401290011.

XU Jianye, WANG Fufang, LIANG Handong, et al. Microstructure Characterization and Mineral Morphology of Tea-Dust Glaze Made in the Ding Kiln of the Northern Song Dynasty[J]. Rock and Mineral Analysis, 2025, 44(1): 115-126. DOI: 10.15898/j.ykcs.202401290011.

北宋定窑茶叶末釉的微观结构与矿物形态学研究

徐建业^{1,2}, 王富芳^{1,2}, 梁汉东^{1,2*}, 李展平^{3,4*}

- (1. 煤炭精细勘探与智能开发全国重点实验室, 北京 100083;
2. 中国矿业大学(北京)地球科学与测绘工程学院, 北京 100083;
3. 清华大学分析中心, 北京 100084;
4. 清华大学化学系, 有机光电子与分子工程教育部重点实验室, 北京 100084)

摘要: 茶叶末釉古瓷作为最早出现的结晶釉之一, 开展深入研究可明确其矿物晶体特征、呈色机理以及古代烧制工艺, 丰富古陶瓷数据库。目前相关研究多来源于二十世纪末, 样本稀少且囊括的年代和窑口严重不足, 所用科学仪器多已淘汰, 亟需更多实验分析与数据支撑。本文采用光学显微镜(OM)、激光剥蚀电感耦合等离子体质谱(LA-ICP-MS)、扫描电镜-能谱(SEM-EDS)、激光共聚焦拉曼光谱(LRS)、飞行时间二次离子质谱(ToF-SIMS)等现代科学仪器对北宋定窑茶叶末釉样本中矿物晶体开展了分析和表征。结果表明, 釉中主晶相与辽金龙泉务窑一致, 为钙长石和辉石; 釉面整体表现为酱-黑色釉基质富铁(Fe_2O_3 含量均值9.73%)和矿物结晶富铁(Fe_2O_3 含量均值11.33%), 除 $\alpha\text{-Fe}_2\text{O}_3$ 和 Fe_3O_4 晶体等熔后重结晶矿物, 还有铁镁尖晶石、残余高岭石等未熔融矿物, 反演出制釉原料中有镁的加入以及烧成温度可能低于1200°C, 异于前人高温烧制的观点。SIMS离子成像揭示了胎釉交界处为厚约20~80 μm 的钙长石晶体层, 而非化妆土或玻璃态的致密反应层。研究揭示了茶叶末古瓷中Fe元素不均匀富集, 部分区域过饱和而析出含铁矿物晶体, 釉面颜色则主要由黄褐色的矿物晶体斑点和酱-黑色玻璃基质共同组成, 同时ToF-SIMS在古瓷微区原位的形貌结构和元素分析上效果显著, 能够辨别钙长石、碱性长石等微米级矿物。

关键词: 茶叶末瓷; 矿物; 元素成像; ToF-SIMS; LA-ICP-MS

要点:

- (1) 茶叶末釉属铁系结晶釉, 表现为黄褐色矿物晶体和酱-黑色釉基质富铁。
- (2) 釉面原料残余的高岭石反演出本研究样本烧成温度可能低于1200°C。
- (3) ToF-SIMS在古陶瓷微区原位上能够实现微米级矿物辨别。

中图分类号: O657.63

文献标识码: A

世界各地还在普遍使用泥盆瓦罐之时, 中国人已经使用上瓷器, 尤以国粹唐宋古瓷闻名。中国古

代结晶釉因烧制过程中析晶不同而形态各异, 却又浑然天成, 备受推崇。茶叶末瓷是中国最早期的

收稿日期: 2024-01-29; 修回日期: 2024-07-12; 接受日期: 2024-07-23; 网络出版日期: 2024-09-06

基金项目: 国家自然科学基金项目(41371449, 41772157); 中央高校基本科研业务费资助项目“太行山东缘煤系地层出露与古窑址分布关系研究”(2022YJSMT01)

第一作者: 徐建业, 硕士研究生, 地质工程专业。E-mail: cheam22@163.com。

通信作者: 梁汉东, 教授, 博士生导师, 主要从事环境科学与风化地球化学等方面的研究工作。
E-mail: HDL6688@vip.sina.com。

通信作者: 李展平, 高级工程师, 主要从事固体材料表面分析、结构表征等研究工作。
E-mail: zhanpingli@mail.tsinghua.edu.cn。

结晶釉,起源于唐代^[1],釉面古朴典雅,耐人寻味。现代关于古陶瓷的科学研究内容包括多个方面,如:釉面的矿物晶体特征^[2]、呈色机理^[3-4]、古代烧制工艺及原料^[5]、古陶瓷的仿造复原^[6]等。对诸如茶叶末等古陶瓷,使用现代前沿的分析仪器进行深入且细致的研究,可加深在古陶瓷制作工艺、呈色机理、分层结构等各方面的认识,为古陶瓷的仿制还原、甄别鉴定、保护修复等方面提供方法原理、研究数据等支撑,弘扬并传承优秀的古瓷文化并促进相关非遗工艺进步。

到目前为止,经过系统研究的古窑口茶叶末瓷釉样本,囊括唐代黄堡窑、浑源窑、观台窑以及辽金时期龙泉务窑,共计12件。唐代茶叶末釉烧成温度控制在1250~1280℃,以还原气氛为主,冷却速度应缓慢,若烧成气氛偏向氧化,颜色会偏褐色^[7];矿物学上黄堡窑和浑源窑茶叶末釉析出的主晶相普通辉石,次晶相为斜长石类(Plagioclase)中的培长石(Bytownite)^[8],而观台窑茶叶末釉主晶相是深绿辉石。辽金时期北京龙泉务窑发现的茶叶末釉中主晶相为普通辉石和钙长石^[9]。不同时期、不同窑口茶叶末釉面中矿物有所区别,源于其原料成分及烧制工艺等多方面的影响,这对分析技术的精确度、适用性等方面都提出更高的要求。如今有多种分析技术已经应用于古陶瓷研究,包括中子活化分析(NAA)、能量色散X射线荧光光谱(EDXRF)、扫描电镜(SEM)、电子探针(EPMA)、飞行时间二次离子质谱(ToF-SIMS)、热电离质谱(TIMs)、激光诱导击穿光谱(LIBS)、激光剥蚀电感耦合等离子体质谱(LA-ICP-MS)、溶液雾化-电感耦合等离子体质谱(SN-ICP-MS)、溶液雾化-电感耦合等离子体发射光谱(SN-ICP-OES)。其中,NAA、TIMs、SN-ICP-MS和SN-ICP-OES等技术在仪器分析之前的样品制备过程中,需要消耗50mg至5g的样品粉末^[10],因此在考古研究中使用受限;虽然EDXRF和EPMA是无损分析技术,但它们的高检测限导致痕量元素测量不够准确^[10]。LA-ICP-MS具备原位、快速、准确、多元素同时检测的分析优势,以及较高灵敏度和空间分辨率成为重要的微区原位元素及同位素测试手段,为地质^[11-12]、冶金^[13]、生物^[14]、材料^[15]、考古^[16]等诸多领域的创新研究提供了重要支撑。ToF-SIMS分析技术具有极高分辨率,可以提供表面、薄膜、界面以至于三维样品的元素、分子等结构信息,具有分析区域小、分析深度浅和不破坏样品的特点^[17]。ToF-SIMS不仅在芯片研发^[18]、宇宙与天

体化学^[19]、地球科学^[20-21]、环境科学^[22-23]、材料科学^[24]、生物医学^[25]等领域广泛应用,还逐渐在考古^[26]、艺术品^[27]、古陶瓷^[28-29]等领域兴起,如徐子琪等^[30]利用ToF-SIMS分析宋代黑釉茶盏油滴,从矿物学角度解释了华北油滴的银色与反光现象。

茶叶末釉古瓷样本数据稀少,需对更多不同窑口、不同历史时期的茶叶末釉样本进行系统物理化学分析,以建立更为全面的茶叶末釉特征数据库。基于前人研究多来源于二十世纪末,本文在借鉴前人对茶叶末古瓷原料、釉面晶体等研究成果的基础上,以北宋定窑茶叶末瓷片为研究对象,利用LA-ICP-MS、ToF-SIMS、SEM-EDS、激光共聚焦拉曼光谱(LRS)等多种谱学仪器和显微观察设备对样本的微观结构、成分和形成机理等进行深入探讨,确定了茶叶末釉微区中矿物的形态、结构、分布及其元素组成。

1 实验部分

1.1 样品与制样

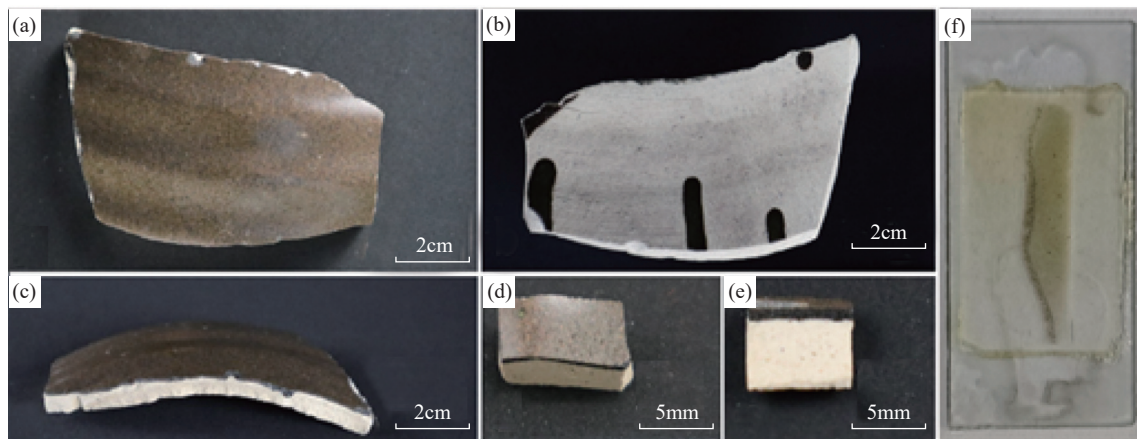
样品是北宋定窑一罐体的腰部残片,其外施茶叶末釉(图1a),内未施釉(图1b);约5mm厚度的胎体呈洁白色泽(图1c),但明显可见铁锈等杂色斑点(图1e),符合定窑采用风化煤矸石(白矸土)亦即“当地出露煤系地层高岭岩风化所成的天然‘高岭泥’”为原料直接制胎的基本特征^[31]。约1mm厚度的釉层截面呈酱-黑色的釉基质(图1e),此色泽与定窑紫金釉以及华北油滴盏的釉基质一致^[30]。

切割样品残片制取1.5cm×1.5cm矩形块并减薄至厚度0.5cm而保留原来釉面作为测试样品A(图1d);制取1.5cm×1.5cm矩形块并按与釉面法线约60°夹角斜切以使可测釉基体“延展”并打磨-抛光,以此作为测试样品B(图1e);另制取3cm×0.5cm矩形块磨平胎底并将截面制备为光学薄片(图1f)。

1.2 样品测试方法

1.2.1 LA-ICP-MS分析

本研究中LA-ICP-MS实验在南京宏创地质勘察技术服务有限公司完成。使用的LA-ICP-MS由193nm深紫外激光剥蚀系统(Resolution SE型,美国Applied Spectra公司)以及电感耦合等离子体质谱仪(Agilent 7900型,美国Agilent公司)组成,配备了S155型双体积样品池。激光参数设置为:束斑直径50μm,剥蚀频率10Hz,能量密度3.5J/cm²,扫描速度3μm/s,通过剥蚀NIST 612标准样品并调节气流,



(a) 残片外侧; (b) 残片内侧; (c) 残片胎; (d) 样本 A; (e) 样本 B; (f) 样本薄片。

图1 宋代茶叶末釉残片

Fig. 1 Tea-dust glaze fragments made in Song Dynasty.

实现了 ^{238}U 的高信号强度(约 $6\times 10^5\text{cps}$)和低氧化物产率($\text{ThO}/\text{Th}<0.2\%$)。同时,使用 $100\mu\text{m}$ 束斑对NIST610进行线扫,以对待测元素进行P/A调谐。分析的质量数涵盖了从 ^{23}Na 到 ^{238}U 的广泛元素,总扫描时间约为0.31s。在样品制备过程中,光片固定于样品支架上,并使用分析纯级别的乙醇擦拭样品表面,去除样品表面可能存在的污染物。对剥蚀区域使用激光脉冲进行预剥蚀(深度约 $1\mu\text{m}$)从而避免污染。最后,在 $50\mu\text{m}$ 束斑直径、5Hz剥蚀频率、 $4.5\text{J}/\text{cm}^2$ 能量密度的条件下对陶瓷样品进行分析。详细的设备调谐参数可参考Thompson等^[32]的工作。

1.2.2 ToF-SIMS 分析

元素成像在清华大学分析中心的飞行时间二次离子质谱仪(ToF SIMS 5-100型,德国ION-TOF GmbH公司)上完成。使用导电胶将样本固定在ToF-SIMS样品台上,在超高真空下用溅射枪对样品表面进行溅射去除表面污染,然后在高质量分辨模式(Spe)和高空间分辨模式(Fast)下采集釉面及胎釉交界处典型区域正、负离子谱。循环时间设置为 $100\mu\text{s}(0\sim 1000\text{amu})$,质量分辨($m/\Delta m$)达到8000,使用电子枪($\pm 20\text{keV}$)对样品表面的荷电效应进行中和处理,以避免对分析结果的干扰。Spe模式参数:一次离子束 Bi^{1+} ,能量 30keV ,束流(脉冲化) 0.8pA ;Fast模式参数:一次离子束 Bi^{1+} ,能量 30keV ,束流(脉冲化) 1.0pA ;溅射参数:溅射枪选择 Ar_n^+ 团簇离子避免溅射束造成表面氧化,能量 10keV ,束流约 9nA 。

1.2.3 SEM-EDS 分析

SEM-EDS(Phenom ProX)对样品进行显微观察。

使用前将样品釉面使用分析级乙醇擦拭清洁后,进行喷铂处理,利用导电胶将样本固定在样品杯上,送入舱中,施加加速电压为 15kV ,电子束电流为 0.6nA 。选择合适区域,直接监测观察表面SEM特征,并进行点和面扫分析。

1.2.4 激光共聚焦拉曼光谱(LRS)分析

矿物物相鉴定使用LRS(HORIBA XploRA Plus)完成,在高放大倍数物镜($\times 100$)下选定测试点,使用激光波长为 638nm ,激光功率 25mW ,光斑直径 $1\mu\text{m}$,扫描范围 $100\sim 1800\text{cm}^{-1}$,曝光时间 $10\sim 100\text{s}$,每个位置扫描2次。

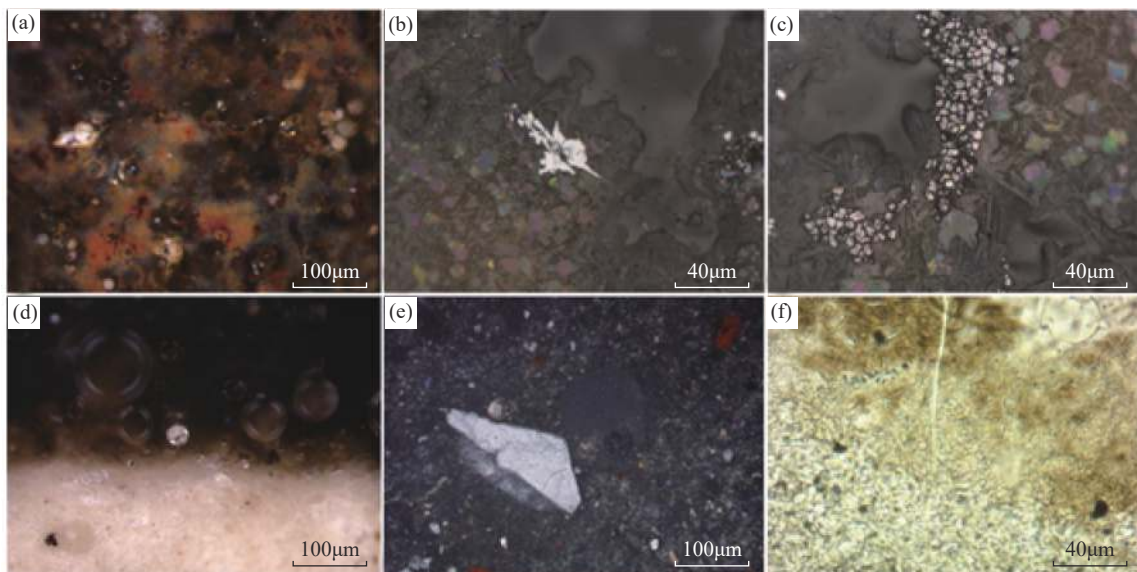
1.3 数据质量控制与数据处理

LA-ICP-MS实验以NIST 610、NIST 612、BCR-2G和BHVO-2G作为标准样品,每10个样品点分析后插入一个标准样品,数据通过使用Iolite软件的“3D Trace Element”方法进行无内标法校正,铁的价态为二价。数据处理包括采集20s的气体空白和35~40s的信号区间。

ToF-SIMS实验数据采用SurfaceLab 7.2软件进行校正、处理和分析,确保获取精确可靠的测试结果。

2 结果与讨论

在光学镜下观察釉面整体分布特征,釉面的主体部分由大面积聚集的黄褐色矿物晶体以及酱-黑色硅铝酸盐基质玻璃组成,少量锈红色斑点散乱分布在釉面,在玻璃基质区域隐约可见大小不一的釉泡聚集,半径约 $10\sim 50\mu\text{m}$ (图2a)。在高倍(200X)镜下可见釉面主晶相呈板片状、针状,单偏光下半自形板



(a) 釉面分布特征; (b) 赤铁矿; (c) 镁铁矿; (d) 胎釉反应层; (e) 胎 (正交偏光); (f) 反应层 (单偏光)。

图2 光学镜下茶叶末瓷中矿物图像

Fig. 2 Optical images of minerals in tea-dust porcelain.

片状晶体大小约为 $15 \sim 35\mu\text{m}$, 表面有彩虹色斑纹, 主要均匀分布在晶体聚集区域中心位置 (图 2 中 b, c); 除主晶相外, 也有部分铁由于过饱和而在釉中析出, 作为晶体相存在, 在单偏光下 (500X) 常见银白色片状金属矿物晶体, 单晶约为 $5 \sim 15\mu\text{m}$, 覆于釉面最表层 (图 2b)。

斜截面镜下可知胎釉交界有厚约 $20 \sim 60\mu\text{m}$ 的墨绿色反应层, 由胎体至釉层颜色逐渐加深, 釉层布满大小不一的釉泡空洞, 半径约 $20 \sim 150\mu\text{m}$, 在釉和胎中可见未完全熔融的石英矿物颗粒和碱性长石, 可在薄片下观察到胎中长石的卡式双晶表面纯净未风化, 有轻微裂纹, 正交偏光下暗红色颗粒为赤铁矿 (图 2 中 d, e), 反应层中可以看到存在微米级针状晶体聚集 (图 2f)。

2.1 元素含量

在茶叶末釉上通过测定釉面斑点和基质的元素组成, 以研究其表面颜色差异的原因。在样品 A 釉

面上分别选择黄褐色斑点与酱黑色基质各 10 个点, 使用 LA-ICP-MS 分析茶叶末釉化学组成, 分别取平均值 (表 1)。釉面以 $\text{SiO}_2\text{-Al}_2\text{O}_3$ 系统为基釉, SiO_2 和 Al_2O_3 含量分别为 56.43% 和 13.22%; CaO 含量 $>10\%$, 为高钙釉。以釉中主要溶剂氧化物种类作为划分类型的基准, 可将茶叶末结晶釉归类于铁系釉, 表现为黑色釉基质富铁 (Fe_2O_3 含量均值 9.73%) 和矿物结晶富铁 (Fe_2O_3 含量均值 11.33%)。

为研究宋代定窑茶叶末瓷样本釉层中元素变化, 在茶叶末瓷斜截面样品 B 上釉层部分选择 4 列, 每列从釉顶至釉底相隔相同距离分别选取 5 个点位, 使用 LA-ICP-MS 分析茶叶末釉中化学组成, 得到 5 行 4 列数据并将每行数据分别取平均值整理为表 2。

2.2 釉面矿物

茶叶末釉颜色多变, 矿物组成复杂, 借鉴火成岩的矿物结晶形成过程、风化过程及以往矿物相关的研究成果, 将釉中矿物晶体按其成因系统划分为熔

表 1 茶叶末釉表面不同颜色斑点元素分析结果

Table 1 Analytical results of elements in different color spots of the tea-dust glaze.

不同颜色斑点	元素含量 (%)									
	Na_2O	MgO	Al_2O_3	SiO_2	K_2O	CaO	TiO_2	Fe_2O_3	P_2O_5	MnO
黄褐色斑点	0.93	1.74	13.99	53.94	3.25	12.09	1.65	11.33	0.88	0.20
酱-黑色基质	0.96	1.58	12.44	58.96	4.03	10.32	1.28	9.73	0.53	0.17
整体	0.94	1.66	13.22	56.43	3.64	11.21	1.47	10.54	0.71	0.18

表 2 茶叶末瓷釉层中元素分析结果

Table 2 Analytical results of elements in glaze layer of tea-dust porcelain.

釉面至釉底 行号	元素含量 (%)									
	Na ₂ O	MgO	Al ₂ O ₃	SiO ₂	K ₂ O	CaO	TiO ₂	Fe ₂ O ₃	P ₂ O ₅	MnO
第 1 行	0.87	1.28	18.36	57.44	3.62	10.29	0.94	6.92	0.16	0.11
第 2 行	0.84	1.68	13.36	59.79	3.84	9.94	1.16	9.05	0.19	0.16
第 3 行	0.87	1.55	13.13	61.50	4.37	9.34	0.92	8.03	0.12	0.15
第 4 行	0.84	1.65	12.59	61.53	4.42	9.18	0.88	8.60	0.14	0.16
第 5 行	0.86	1.65	13.51	60.63	3.88	9.66	0.93	8.60	0.12	0.16

后重结晶矿物、未熔融矿物、风化成因矿物三大类。

2.2.1 熔后重结晶矿物

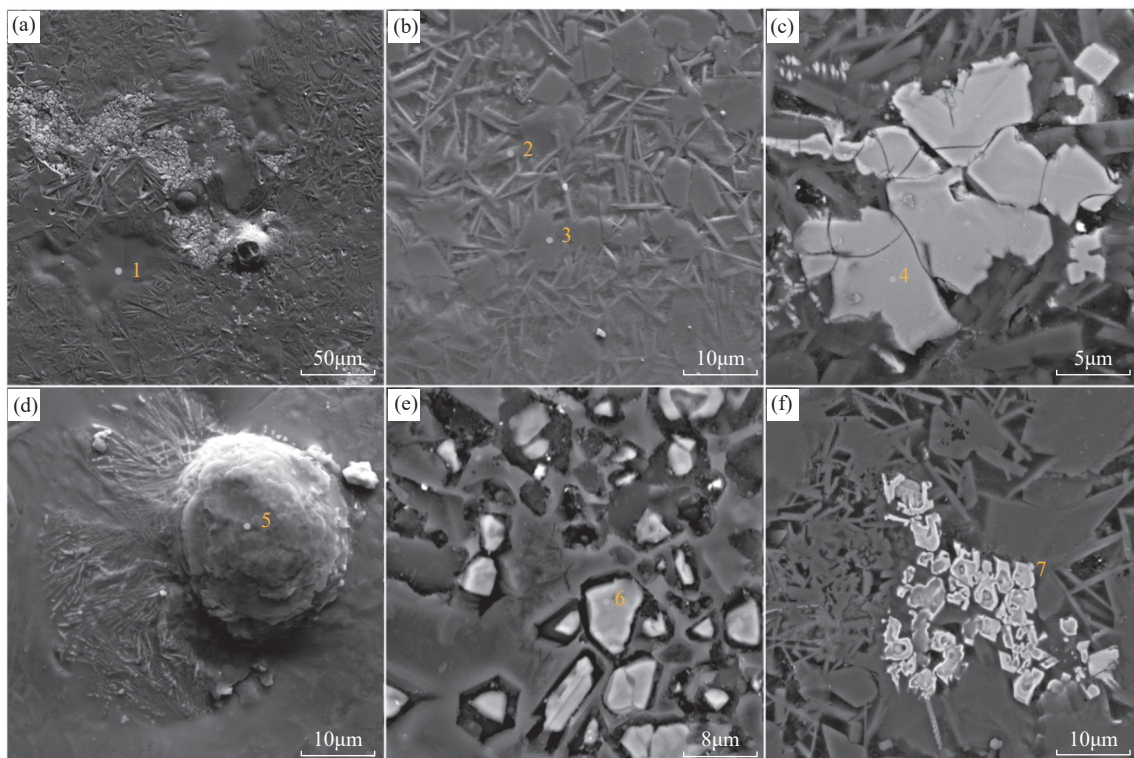
熔后重结晶矿物是釉料在烧制的过程中熔融后再冷却重结晶形成, 最明显的特征为晶面的发育程度好, 多为自形晶。根据烧制气氛的控制、饱和度高低和冷却速度快慢, 所形成矿物晶体的种类、大小和形态亦不同, 本文详细报道重结晶矿物有莫来石、钙长石、赤铁矿、 ϵ -Fe₂O₃、金红石、辉石等矿物^[33-35]。

使用 SEM 对样本釉面矿物进行表征(图 3), 并对图 3 中标记点位使用 EDS 显示元素组成(表 3)。

釉面针状晶体相对板片状晶体分布更广, 除聚

集区域中心处与板片状晶体交杂, 还分布于聚集体边缘处, 呈杂乱无规则状, 晶体在中心处长约 10~40 μ m, 边缘处约 30~120 μ m。BSE 模式下图像显示, 釉玻璃基质上方铺陈针状晶体, 板片状晶体则覆盖在针状晶体上方, 整体上此区域基质显露约 10%, 针状占 40%, 板片状约占 60%(图 3 中 a, b)。点 1 为玻璃基质; 点 2、3 分别为针状、板片状矿物, 由元素占比可知为长石和普通辉石, 与金元时期旬邑茶叶末瓷、主晶系相同^[9,36]。

釉面银白色片状金属矿物(图 3c)主要元素组成为 Fe, 拉曼光谱测试谱图示于图 4, 图中 228、350、



(a) 釉面分布特征; (b) 主晶相; (c) 赤铁矿; (d) 高岭石; (e) 镁铁矿; (f) 含钛磁铁矿。

图 3 扫描电镜下茶叶末瓷中矿物图像

Fig. 3 Images of minerals in tea-dust porcelain by SEM.

表 3 EDS 下矿物晶体元素组成

Table 3 Elemental composition of mineral crystals under EDS.

EDS 所取点位	元素原子占比 (at%)									
	Si	Al	Ca	Fe	Mg	K	Na	Cr	Ti	Mn
1	63.67	13.8	8.14	3.97	3.61	4.85	1.96	/	/	/
2	60.59	21.39	7.99	2.08	2.48	1.07	4.22	/	/	0.18
3	51.53	25.74	13.82	3.83	1.6	1.13	2.35	/	/	/
4	5.61	2.18	1.26	89.71	/	0.98	/	/	/	/
5	41.2	34.14	3.26	4.79	4.37	2.78	3.03	/	5.87	/
6	1.85	/	0.43	65.59	29.93	0.23	/	1.96	/	/
7	11.78	6.5	/	77.79	/	/	/	/	3.92	/

注：元素原子占比低于 0.10at% 以“/”表示。

601、672、1328 cm^{-1} 为主要位移峰，与赤铁矿 ($\alpha\text{-Fe}_2\text{O}_3$) 晶体在拉曼标准谱库中谱图一致。这些特征峰也出现在宋代黑釉油滴盏、华北山西临汾窑等 $\alpha\text{-Fe}_2\text{O}_3$ 晶体的拉曼谱图中^[30, 37]，同为铁元素饱和析出的重结晶矿物，宋代油滴形态上为近百余枚银色六方柱晶体自组织分散排列构成，而临汾窑的铁锈斑则为许多深红色多边形晶体组成。

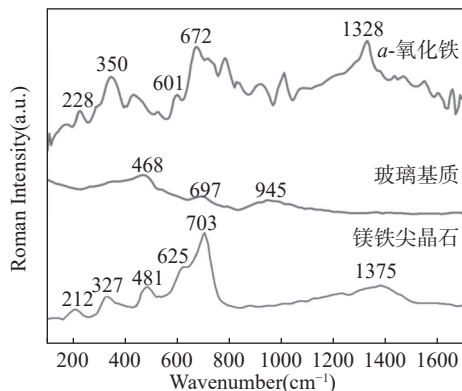


图 4 样本的拉曼图谱

Fig. 4 Raman spectra of the samples.

2.2.2 未熔融矿物

釉中部分矿物因高熔点，烧制过程中部分未熔融或未完全熔融，这些矿物来自釉料，依然保持烧制前的特性，常见的有石英、磁铁矿、长石和黏土矿物^[9]。

扫描电镜下样本釉面发现未完全熔融黏土矿物颗粒，黏土矿物颗粒圆滑呈球状，同时可见层状堆叠结构，且仅一小部分发生熔融 (图 3d)，使用 EDS 测定化学成分主要元素为 Si、Al，且其 Si/Al 的原子比介于 1.1 ~ 1.3，判断未完全熔融黏土矿物为釉料携带的高岭石。

釉面观察到一种未熔融矿物异于其他矿物，部分晶体颗粒在外界条件作用下已脱落，留下凹坑，部分晶体破碎，半自形状，磨圆度一般，大小为 1 ~ 5 μm (图 3e)。此矿物颗粒直接嵌入玻璃基质中而非铺陈其上，显然不是熔融后冷却结晶形成，而是残留相，EDS 显示该矿物主要元素组成为 Fe 和 Mg。此晶体的拉曼谱图谱峰显示主位移峰为 212、327、481、625、703、1375 cm^{-1} ，与 Renishaw 矿物和无机材料数据库 (RMIM No.503)、RRuFF 数据库 (RRuFF ID: R070127) 中合成氧化镁铁素体的标准拉曼光谱进行比较，为镁铁矿 (MgFe_2O_4) 特征峰，又称为镁铁尖晶石 (图 4)。该矿物在宋代耀州窑酱黑釉中首次被证实存在，酱黑釉中镁铁矿除富铁、富镁外，还富钙^[38]；在宋金时期浑源窑黑釉剔花瓷片也发现了大量镁铁矿晶体，为棕黄色树枝状^[39]。

2.2.3 风化成因矿物

瓷器烧制完成后，釉面矿物长时间暴露在空气中或埋藏于地下，在风化作用下发生氧化还原、破坏和分解，从而会形成一些衍生矿物，主要存在于釉面表层及裂隙、机械损伤处，常见的衍生矿物为碳酸钙、高岭石、赤铁矿等，严重风化情况下表现为釉面腐蚀^[35]。

图 3f 中不规则粒状、鳞片状晶体，单晶约为 1 ~ 5 μm ，EDS 显示矿物主要元素组成为 Fe，晶体中少量 Ti 取代 Fe，根据元素组成和单晶形态，为含钛磁铁矿，三方晶系，晶体边缘为白色环状。

未被交代的粒状磁铁矿在扫描电镜背散射测试下表面几乎不存在孔隙，而被交代的磁铁矿和交代形成的假象赤铁矿表面的孔隙会明显增多，且粒状假象赤铁矿表面孔隙多于板状赤铁矿^[40]。釉面长期与空气接触，磁铁矿在风化作用下，边缘或破碎处

易被氧化,生成赤铁矿,进一步判断该晶体为未完全被赤铁矿交代的含钛磁铁矿。

2.3 胎釉反应层

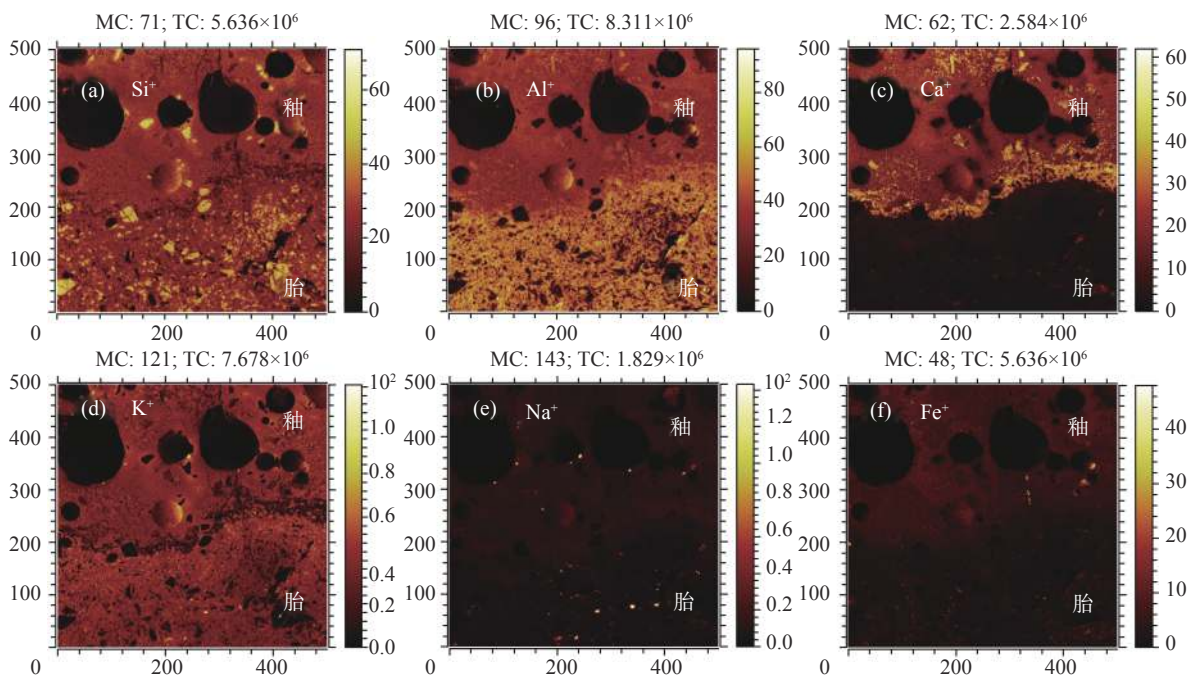
斜截面胎釉交界处反应层的 ToF-SIMS $500\mu\text{m}\times 500\mu\text{m}$ 正离子图像如图 5 所示。其中 Si^+ 离子图像中,胎中石英颗粒明显高于釉中,大小约为 $1\sim 20\mu\text{m}$; 茶叶末釉属于钙质釉或钙碱釉,因此 Ca^+ 离子图像可以明显区别出釉、胎以及反应层,胎釉交界处针状晶体层丛生,晶体主要元素为 Ca^+ 、 Al^+ 、 Si^+ 离子,含有少部分 Na^+ 离子,为斜长石亚类中钙长石,而非碱性长石,这是由于釉中碱土金属氧化物 ($\text{CaO}+\text{MgO}$) 含量远高于碱金属氧化物 ($\text{Na}_2\text{O}+\text{K}_2\text{O}$)。 Ca^+ 、 Fe^+ 离子图像显示,针状晶体不仅存在于胎釉交界处,还大量赋存于釉中,与气泡附近 Fe^+ 含量较高区域互衬。 Na^+ 成像中的黄亮色光点同时位于 K^+ 、 Si^+ 、 Al^+ 成像范围上,为胎釉中未完全熔融的碱性长石。

2.4 茶叶末釉的呈色机理与烧制工艺要点

茶叶末釉的黄褐色斑点和酱-黑色玻璃基质共同表现出釉面颜色以及釉面相对的粗糙度。黄褐色斑点中 Ca 、 Fe 含量较高,釉中 CaO 的存在能够改善釉面的光泽度且析出的钙长石有助于提高乳浊效果,同时 Fe 是茶叶末釉中的最主要着色元素,在 Fe 和 Ca 元素的共同作用下,富集 Fe 、 Ca 的硅铝酸盐晶体

堆积在一起宏观上表现为釉表面细小的黄褐色似茶沫颗粒。酱-黑色玻璃基质中 Si 、 K 含量较高,这是由于富 K 原料主要为天然碱性长石,常为固溶体,熔点较单一成分的长石熔点低,具有良好的助熔作用, $\text{Al}_2\text{O}_3\text{-SiO}_2$ 体系中加入长石,则可在 $985\pm 20^\circ\text{C}$ 即开始出现液相,且长石含量越高,初熔温度越低^[41],故 K^+ 一般分布于釉基质中,其二次离子图像可以表现出釉基质的分布特征。釉层元素分布表现出明显差异性, Fe 在釉面最低,在釉中最高,结合 Fe^+ 的二次离子图像,这可能是烧制过程中气泡携带 Fe 向上悬浮,由于釉浆流动性较差加上快速冷却,大量气泡悬停在釉中区域,导致 Fe 在此最高,在釉面最低。

高岭石作为烧制瓷器的主要黏土矿物,在 1200°C 左右会形成莫来石晶体,在釉料中助溶剂的作用下,熔融温度则会进一步降低,未熔融矿物类的残余高岭石矿物球粒反演出本研究样本的烧成温度很可能低于 1200°C ,区别于目前关于耀州窑等唐宋茶叶末釉属于高温釉的看法。同为未熔融矿物类中的铁镁尖晶石 ($\text{MgFe}_2^{3+}\text{O}_4$) 熔点为 1713°C ,首次见于茶叶末釉,作为原始釉料携带物,可在后续研究中通过其携带的稀土元素和同位素等信息进行有效的地球化学示踪,并能够对岩石矿物的成因、演化和来源分析提供帮助^[42]。



MC 为单个像素点最大计数; TC 为总计数。

图5 胎釉截面 $500\mu\text{m}\times 500\mu\text{m}$ 二次离子图像

Fig. 5 Secondary ion images of the section of the body and glaze.

3 结论

利用 LA-ICP-MS、ToF-SIMS、SEM-EDS 等技术方法,确定了北宋定窑茶叶末釉微区中矿物的形态、结构、分布及其元素组成。属高钙釉、铁系结晶釉,表现为酱-黑色釉基质富铁 (Fe_2O_3 含量均值 9.73%) 和黄褐色矿物结晶富铁 (Fe_2O_3 含量均值 11.33%),同时 Fe 在釉层中分布不均,在釉面最低,釉中最高。釉面矿物簇群据各自元素组成和形貌特征区分为三类,熔后重结晶形成的钙长石和辉石作为主晶相矿物,与辽金龙泉窑一致;茶叶末釉的颜色在很大程度上归因于其析出的辉石类晶体(镁铁类矿物),充足的 MgO 是烧制茶叶末釉的关键因素,镁铁矿指示出当时制釉原料中已有镁的引入;烧制温度作为另一关键因素,前人研究认为唐宋茶叶末釉应处于 1250 ~ 1280 °C,然而原始釉料中残余的高岭

石球粒矿物则反映出该茶叶末瓷烧成温度可能低于 1200 °C。

在古陶瓷研究过程中,为有效地避免珍贵样品被破碎^[16],目前已有使用 LA-ICP-MS 测定大尺寸陶瓷主微量元素组成方法的案例。同属于非破坏性分析,ToF-SIMS 在样本尺寸选择上虽仍有一定局限,但作为前沿实用的表面分析技术之一,在古瓷的微区原位研究方面有着明显的优势,形貌结构与元素分布表现优秀,能够辨别钙长石、碱性长石等微米级矿物。ToF-SIMS 和 LA-ICP-MS 等测试方法可望运用于国粹唐宋古瓷的研究和甄别,以促进相关非遗工艺进步。

致谢: 感谢南京宏创地质勘察技术服务有限公司武现伟老师在 LA-ICP-MS 实验上提供的帮助。

Microstructure Characterization and Mineral Morphology of Tea-Dust Glaze Made in the Ding Kiln of the Northern Song Dynasty

XU Jianye^{1,2}, WANG Fufang^{1,2}, LIANG Handong^{1,2*}, LI Zhanping^{3,4*}

(1. State Key Laboratory for Fine Exploration and Intelligent Development of Coal Resources, Beijing 100083, China;

2. College of Geoscience and Surveying Engineering, China University of Mining and Technology (Beijing), Beijing 100083, China;

3. Key Laboratory of Organic Optoelectronics and Molecular Engineering of Ministry of Education Department of Chemistry, Tsinghua University, Beijing 100084, China;

4. Analysis Center Tsinghua University, Tsinghua University, Beijing 100084, China)

HIGHLIGHTS

- (1) Tea-dust glaze belongs to the iron system of crystallization glaze, which is manifested as tan mineral crystals and sauce-black glaze matrix rich in iron.
- (2) The residual kaolinite of glazed raw materials shows that the firing temperature of the samples in this study was most likely below 1200 °C.
- (3) ToF-SIMS can distinguish micron-level mineral discrimination *in situ* on ancient ceramics.

ABSTRACT: The tea-dust glaze ancient porcelain is one of the earliest crystalline glazes, which is rarely studied deeply because of its rarity. In this study, the mineral crystals in tea-dust glaze made in the Ding Kiln of the Northern Song Dynasty were analyzed by optical microscope (OM), laser ablation-inductively coupled plasma-mass spectrometry (LA-ICP-MS), scanning electron microscopy coupled with an X-ray energy dispersive spectrometer (SEM-EDS), laser confocal Raman spectrometer (LRS), and high-resolution time of flight-secondary ion mass spectrometry (ToF-SIMS). The results show that the main crystal phase in the glaze is the same as that of the

Longquanwu Kiln in the Liao and Jin Dynasty, which is anorthite and augite. The overall performance of the glaze is that the sauce-black glaze matrix is rich in iron (Fe_2O_3 mean 9.73%) and the mineral crystal is rich in iron (Fe_2O_3 mean 11.33%). In addition to $\alpha\text{-Fe}_2\text{O}_3$ crystals, Fe_3O_4 crystals and other recrystallized minerals after melting, the glaze also has pleonaste, residual kaolinite and other unmelted minerals from raw glaze materials. The residual kaolinite shows that the firing temperature of the samples in this study was most likely below 1200°C. The BRIEF REPORT is available for this paper at <http://www.ykcs.ac.cn/en/article/doi/10.15898/j.ykcs.202401290011>.

KEY WORDS: tea-dust glaze; minerals; element imaging; ToF-SIMS; LA-ICP-MS

BRIEF REPORT

Significance: Modern scientific research on ancient ceramics encompasses numerous aspects, such as the mineral crystal characteristics of the glaze^[2], the color mechanism of the glaze^[3], the ancient firing process and raw materials^[5], and the reproduction and restoration of ancient ceramics^[6]. The utilization of modern cutting-edge analytical instruments to conduct in-depth and detailed research on ancient ceramics, such as tea-dust porcelain, can enhance the understanding of the production process, color mechanism, layered structure and other aspects of ancient ceramics. It cannot only offer methods, principles, research data and other supports for the imitation and restoration, identification, protection and restoration of ancient ceramics, but also promote and inherit the outstanding ancient porcelain culture and advance the progress of related intangible cultural heritage.

As one of the earliest crystallized glazes, to date, 12 samples of tea-dust glaze from ancient kilns have been systematically investigated, including the Huangbao Kiln in the Tang Dynasty, the Hunyuan Kiln, the Guantai Kiln and the Longquanwu Kiln in the Liao and Jin Dynasties^[7-9]. With the deepening of research on ancient ceramics, the importance of minerals has become increasingly prominent, but there is still a lack of directional classification of minerals in this field. At the same time, the majority of the scientific instruments employed have been phased out, and more experimental analysis and data support are urgently needed to establish a more comprehensive database of tea-dust glaze characteristics.

In this research, tea-dust glaze pieces of the Ding Kiln in the Northern Song Dynasty were studied by LA-ICP-MS, ToF-SIMS, SEM-EDS and LRS. Drawing on the mineral crystallization and weathering processes of igneous rocks and previous mineral related research results, for the first time, mineral crystals in ceramic glazes were classified into three categories based on their genesis system: post melting recrystallized minerals, unmelted minerals, and weathering minerals. The different classification minerals were revealed to have different indicative meanings for ceramic research. The tea-dust glaze belonged to the iron system of crystallization glaze, which was manifested as tan mineral crystals and sauce-black glaze matrix rich in iron. The residual kaolinite of glazed raw materials shows that the firing temperature of the sample was most likely below 1200°C, which was different from the current view that the tea-dust glaze of Tang and Song such as the Yaozhou Kiln belonged to high-temperature glaze.

Methods: (1) Sample information. The sample is the waist fragment of a pot from the Ding Kiln of the Northern Song Dynasty. The exterior is coated with tea glaze (Fig.1a), while the interior is unglazed (Fig.1b). The body, approximately 5mm thick and white in color (Fig.1c), exhibits distinct spots of rust and other colors (Fig.1e). This is in accordance with the fundamental characteristics of direct tire production by Dingyao, using weathered coal gangue (white dirt) as a raw material^[31]. The cross section of the glaze layer, approximately 1mm thick, presents a sauce-black glaze matrix (Fig.1e). A 1.5cm×1.5cm rectangular block was fabricated by cutting the sample fragments and thinned to a thickness of 0.5cm, while the original glaze was retained as test sample A (Fig.1d). Another 1.5cm×1.5cm rectangular block was produced and beveled at an angle of approximately 60° from the normal of the enamel surface to “extend” the matrix of the measured glaze, and then polished as test sample B (Fig.1e).

Additionally, a 3cm×0.5cm rectangular block was made to smooth the tire base and the section was fabricated into an optical slice (Fig.1f).

(2) LA-ICP-MS analyses. LA-ICP-MS consists of a 193nm deep ultraviolet laser denudation system (Applied Spectra's Resolution SE) and an inductively coupled plasma mass spectrometer (Agilent's Agilent 7900). Laser parameters are set as follows: spot diameter 50μm, denudation frequency 10Hz, energy density 3.5J/cm², scanning speed 3μm/s. Detailed equipment tuning parameters can be found in Thompson et al.^[32]. NIST610, NIST612, BCR-2G and BHVO-2G were used as standard samples, and the standard sample was inserted after every 10 sample points for analysis. The data were corrected by the "3D Trace Element" method using Iolite software without an internal standard method, and the valence state of iron was bivalent.

(3) ToF-SIMS analyses. ToF-SIMS (TOF SIMS 5-100, ION-TOF GmbH, Germany) was set with a cycle time of 100μm (0–1000amu). A sputtering gun was used to remove sample surface contamination, and an electron gun (±20keV) was used to neutralize the charge effect on the sample surface. Spe mode parameters: an ion beam Bi1⁺, energy 30keV, beam (pulsed) 0.8pA; fast mode parameters: an ion beam Bi1⁺, energy 30keV, beam (pulsing) 1.0pA. Sputtering parameters: the sputtering gun chooses Ar_n⁺ cluster ions to avoid surface oxidation caused by the sputtering beam, with an energy of 10keV and a beam current of about 9nA. SurfaceLab 7.2 software was used to correct and analyze the ToF-SIMS experimental data.

(4) SEM-EDS analyses. Before the use of SEM-EDS (Phenom ProX), the sample glaze was wiped and cleaned with analytical grade ethanol, and then sprayed with platinum. The accelerated voltage was 15kV and the electron beam current was 0.6nA.

(5) LRS analyses. Mineral phase identification was completed by using LRS (HORIBA XploRA Plus). The test point was selected under a high-magnification objective (×100). The laser wavelength was 638nm, the laser power was 25mW, the spot diameter was 1μm, the scanning range was 100–1800cm⁻¹, and the exposure time was 10-100s. Each location was scanned twice.

Data and Results: The sample is of a high calcium glaze (CaO content>10%), and also an iron crystalline glaze. The overall performance of the glaze matrix is a sauce-black iron-enriched (Fe₂O₃ content mean of 9.73%) and yellow-brown mineral crystal iron-enriched (Fe₂O₃ content mean of 11.33%). The mineral clusters can be classified into three types based on their elemental composition and morphological characteristics. The main crystalline minerals are anorthite and augite formed through recrystallization after melting, which are consistent with those of the Longquanwu Kiln in the Liao and Jin Dynasties. The Raman spectra of α-Fe₂O₃ crystals precipitated by saturated iron elements are in accordance with those of the black glaze Huabei oil in the Song Dynasty and the Linfen Kiln in Shanxi^[30,37]. Residual kaolinite as an unmelted mineral was detected in the glaze, which indicates that the sintering temperature is lower than 1200°C. SIMS ion imaging indicated that Fe was not uniformly enriched near the glaze bubble, and there was a 20–80μm thick anorthite crystal layer at the fetal glaze junction, rather than a dense reaction layer in the makeup clay or glass state.

参考文献

- [1] 陈代璋, 袁家铮, 刘光辉. 结晶釉的绿辉石研究[J]. *地质论评*, 1996, 42(2): 129–135.
Chen D Z, Yuan J Z, Liu G H. Green pyroxene studies of crystalline glazes[J]. *Geological Review*, 1996, 42(2): 129–135.
- [2] Tao S, Liu S, Yuan Y, et al. Micro-structural and compositional study: ε-Fe₂O₃ crystals in the Hare's Fur Jian Ware[J]. *Crystals*, 2022, 12(3): 367–371.
- [3] Wen R, Wang D, Wang L H, et al. The colouring mechanism of the Brown glaze porcelain of the Yaozhou Kiln in the Northern Song Dynasty[J]. *Ceramics International*, 2019, 45(8): 10589–10595.
- [4] Chen X Y, Li W D, Xu C S, et al. Angle dependence of Jian bowl color and its coloring mechanism[J]. *Journal of the European Ceramic Society*, 2022, 42(2): 693–706.
- [5] Wu B, Zhao W, Ren X, et al. Firing process and colouring mechanism of black glaze and brown glaze porcelains from the Yuan and Ming dynasties from the Qingliang Temple kiln in Baofeng, Henan, China[J].

- Ceramics International*, 2021, 47(23): 32817–32827.
- [6] Li X Y, Lu J H, Yu X L, et al. Imitation of ancient black-glazed Jian bowls (Yohen Tenmoku): Fabrication and characterization[J]. *Ceramics International*, 2016, 42(14): 15269–15273.
- [7] 黄瑞福, 陈显求, 陈士萍, 等. 唐代茶叶末瓷的物理化学基础研究[J]. *陶瓷学报*, 1993, 14(2): 11–20.
Huang R F, Chen X Q, Chen S P, et al. The physico-chemistry investigation on Tang Dynasty tea dust porcelain[J]. *Journal of Ceramics*, 1993, 14(2): 11–20.
- [8] 张福康. 中国古陶瓷的科学[M]. 上海: 上海人民美术出版社, 2000: 82–91.
- [9] 陈尧成, 张筱薇, 黄秀纯, 等. 北京龙泉窑辽金代黑瓷的制作工艺和显微结构研究[J]. *中国陶瓷*, 1999, 35(6): 38–42.
Chen Y C, Zhang X W, Huang X C, et al. Study on microstructure and technology of black porcelain of Beijing Longouanwu Kiln in Liao and Jin Dynasties[J]. *China Ceramics*, 1999, 35(6): 38–42.
- [10] Bao Z A, Yuan H L, Wen R, et al. The fast and direct characterization of blue-and-white porcelain glaze from Jingdezhen by laser ablation-inductively coupled plasma mass spectrometry[J]. *Analytical Methods*, 2015, 7(12): 5034–5040.
- [11] 何旭科, 栾燕, 孙晓辉, 等. 辽宁弓长岭铁矿床蚀变围岩中石榴石 LA-ICP-MS 面扫描分析及元素分布特征[J]. *岩矿测试*, 2023, 42(4): 707–720.
He X K, Luan Y, Sun X H, et al. LA-ICP-MS Mapping and element distribution characteristics of garnet from the altered wall-rock of the Gongchangling iron deposit in Liaoning Province[J]. *Rock and Mineral Analysis*, 2023, 42(4): 707–720.
- [12] 何焘, 张晨西, 张文, 等. 高空间分辨率 LA-ICP-MS 测定硅酸盐玻璃标准物质中 42 种微量元素[J]. *岩矿测试*, 2023, 42(5): 983–995.
He T, Zhang C X, Zhang W, et al. Determination of 42 trace elements in silicate glass reference materials by high spatial resolution LA-ICP-MS[J]. *Rock and Mineral Analysis*, 2023, 42(5): 983–995.
- [13] 陈晓峰, 胡芳菲, 张煦, 等. 激光剥蚀-电感耦合等离子体质谱法测定纯铜中铁锌砷锡铅铋[J]. *冶金分析*, 2018, 38(12): 1–6.
Chen X F, Hu F F, Zhang X, et al. Determination of iron, zinc, arsenic, tin, antimony, lead and bismuth in pure copper by laser ablation inductively coupled plasma mass spectrometry[J]. *Metallurgical Analysis*, 2018, 38(12): 1–6.
- [14] 付东旭, 郑令娜, 刘金辉, 等. 激光剥蚀-电感耦合等离子体质谱定量分析单细胞中的银纳米颗粒[J]. *分析化学*, 2019, 47(9): 1390–1394.
Fu D X, Zheng L N, Liu J H, et al. Quantitative analysis of silver nanoparticles in single cell by laser ablation inductively coupled plasma-mass spectrometry[J]. *Chinese Journal of Analytical Chemistry*, 2019, 47(9): 1390–1394.
- [15] 赵峰, 王占明, 王挺, 等. 激光剥蚀电感耦合等离子体质谱 (LA-ICP-MS) 法测定涂层氧化锆颗粒铌层中 24 种微量杂质元素[J]. *中国无机分析化学*, 2023, 13(4): 374–381.
Zhao F, Wang Z M, Wang T, et al. Determination of 24 trace impurities in niobium coating of zirconia particles by laser ablation inductively coupled plasma mass spectrometry (LA-ICP-MS)[J]. *Chinese Journal of Inorganic Analytical Chemistry*, 2023, 13(4): 374–381.
- [16] 周帆, 李明, 柴辛娜, 等. 非破坏性开放式激光剥蚀电感耦合等离子体质谱法原位测定大尺寸陶瓷样品主微量元素组成[J]. *岩矿测试*, 2021, 40(1): 33–41.
Zhou F, Li M, Chai X N, et al. *In-situ* non-destructive determination of major and trace elements in large size ceramic samples by open laser ablation inductively coupled plasma-mass spectrometry[J]. *Rock and Mineral Analysis*, 2021, 40(1): 33–41.
- [17] 李展平. 飞行时间二次离子质谱 (TOF-SIMS) 分析技术[J]. *矿物岩石地球化学通报*, 2020, 39(6): 1173–1190.
Li Z P. Time-of-flight secondary ion mass spectrometry[J]. *Bulletin of Mineralogy, Petrology and Geochemistry*, 2020, 39(6): 1173–1190.
- [18] 阿尔弗来德·贝宁豪文, 查良镇. 飞行时间二次离子质谱—强有力的表面、界面和薄膜分析手段[J]. *真空*, 2002(5): 10–14.
Benninghoven A, Zha L Z. TOF-SIMS—A powerful tool for practical surface, interface and thin film analysis[J]. *Vacuum*, 2002(5): 10–14.
- [19] Timms N E, Kirkland C L, Cavosie A J, et al. Shocked titanite records Chicxulub hydrothermal alteration and impact age[J]. *Geochimica et Cosmochimica Acta*, 2020, 281: 12–30.
- [20] 梁汉东. 金/硫团簇非共价键相互作用的研究与意义[J]. *中国矿业大学学报*, 2001, 30(6): 593–599.
Liang H D. Investigation into non-covalent interaction between gold and sulfur clusters by TOF-SIMS[J]. *Journal of China University of Mining & Technology*, 2001, 30(6): 593–599.
- [21] 梁汉东, 刘敦一. 金硫团簇负离子组成特征的探讨[J]. *物理化学学报*, 2001, 17(9): 859–864.
Liang H D, Liu D Y. Compositional and constitutional characterization of Au-S cluster ions[J]. *Acta Physico-Chimica Sinica*, 2001, 17(9): 859–864.
- [22] Liang H D. Secondary ion mass spectrometry of high-sulfur coal: Observation and interpretation of polysulfur ions[J]. *Chinese Science Bulletin*, 1999, 44(13): 1242–1245.
- [23] Liang H D, Liang Y C, Gardella J A, et al. Potential

- release of hydrogen fluoride from domestic coal in endemic fluorosis area in Guizhou, China[J]. *Chinese Science Bulletin*, 2011, 56(22): 2301–2303.
- [24] Zhang T, Meng X, Bai Y, et al. Profiling the organic cation-dependent degradation of organolead halide perovskite Solar cells[J]. *Journal of Materials Chemistry A*, 2017, 5(3): 1103–1111.
- [25] White L J, Taylor A J, Faulk D M, et al. The impact of detergents on the tissue decellularization process: A ToF-SIMS study[J]. *Acta Biomaterialia*, 2017, 50: 207–219.
- [26] 刘婕, 陈相龙, 梁汉东, 等. 新疆汉代羊毛织物染料的飞行时间二次离子质谱表征[J]. *质谱学报*, 2024, 45(3): 386–395.
- Liu J, Chen X L, Liang H D, et al. Characterization of dyes for Han Dynasty wool fabrics in Xinjiang by time-of-flight secondary ion mass spectrometry[J]. *Journal of Chinese Mass Spectrometry Society*, 2024, 45(3): 386–395.
- [27] Ingo G M, Riccucci C, Pascucci M, et al. Combined use of FE-SEM plus EDS, ToF-SIMS, XPS, XRD and OM for the study of ancient gilded artefacts[J]. *Applied Surface Science*, 2018, 446: 168–176.
- [28] Kaluzna-czaplinska J, Rosiak A, Grams J, et al. The studies of archaeological pottery with the use of selected analytical techniques[J]. *Critical Reviews in Analytical Chemistry*, 2017, 47(6): 490–498.
- [29] Felicissimo M P, Peixoto J L, Bittencourt C, et al. SEM, EPR and ToF-SIMS analyses applied to unravel the technology employed for pottery-making by pre-colonial Indian tribes from Pantanal, Brazil[J]. *Journal of Archaeological Science*, 2010, 37(9): 2179–2187.
- [30] 徐子琪, 赵焯赫, 梁汉东, 等. 宋代黑釉茶盏油滴的飞行时间二次离子质谱表征[J]. *质谱学报*, 2023, 44(1): 25–33.
- Xu Z Q, Zhao X H, Liang H D, et al. Characterization of oil spots on black-glazed teabowl made in Song Dynasty by time-of-flight secondary ion mass spectrometry[J]. *Journal of Chinese Mass Spectrometry Society*, 2023, 44(1): 25–33.
- [31] 刘婕, 梁汉东. 华北唐宋古瓷窑兴起的自然条件: 煤系地层出露[J]. *中国煤炭地质*, 2024, 36(1): 12–17.
- Liu J, Liang H D. Natural condition for the rise of ancient porcelain kilns of the Tang and Song Dynasties in North China: Outcrops of coal strata[J]. *Coal Geology of China*, 2024, 36(1): 12–17.
- [32] Thompson J M, Meffre S, Danyushevsky L. Impact of air, laser pulse width and influence on U-Pb dating of zircons by LA-ICPMS[J]. *Journal of Analytical Atomic Spectrometry*, 2018, 33: 221–230.
- [33] 顾幸勇, 方豪, 宋仪杰. 茶叶末结晶釉主晶相的研究[J]. *中国陶瓷*, 1989, 25(2): 6–9.
- Gu X Y, Fang H, Song Y J. A study on principal crystalline phase of tea-dust crystalline glaze[J]. *China Ceramics*, 1989, 25(2): 6–9.
- [34] Li W, Luo H, Li J, et al. Studies on the microstructure of the black-glazed bowl sherds excavated from the Jian Kiln site of ancient China[J]. *Ceramics International*, 2008, 34(34): 1473–1480.
- [35] Ma Q L, Xu S Q, Wang J L, et al. Integrated analysis of a black-glazed porcelain bowl in Tushan Kiln dated back to Song Dynasty, China[J]. *Materials Chemistry and Physics*, 2020, 242: 122213.
- [36] 陈显求, 陈士萍, 周学林, 等. 金、元时期旬邑窑茶叶末瓷的研究[J]. *陶瓷学报*, 1996, 17(3): 15–24.
- Chen X Q, Chen S P, Zhou X L, et al. The study on Jin and Yuan Dynasties tea dust wares from Xunyi Kiln Site[J]. *Journal of Ceramics*, 1996, 17(3): 15–24.
- [37] Wang M, Wang T, Wang F, et al. Raman study of rusty oil spotted glaze produced in Linfen Kilns (Shanxi Province, AD1115–1368)[J]. *Journal of Raman Spectroscopy*, 2020, 53(3): 582–592.
- [38] Wang T, Hole C, Ren Z, et al. Morphological and structural study of crystals in black-to-brown glazes of Yaozhou ware (Song Dynasty) using imaging and spectroscopic techniques[J]. *Journal of the European Ceramic Society*, 2021, 41(12): 6049–6058.
- [39] 王秀玲, 侯亮亮, 王敏力, 等. 山西大同浑源窑出土黑釉剔花瓷片的科技分析[J]. *中国陶瓷*, 2022, 58(8): 53–58.
- Wang X L, Hou L L, Wang M L, et al. Scientific and technological analysis of black-glazed carving ware of Hunyuan Kilns in Datong, Shanxi Province[J]. *China Ceramics*, 2022, 58(8): 53–58.
- [40] 付玲芝. 辽宁省弓长岭铁矿磁铁矿-赤铁矿转变机制研究[D]. 长春: 吉林大学, 2016: 58–62.
- Fu L Z. Study on mechanism of transforming between magnetite and hematite of Gongchangling iron deposit in Liaoning Province[D]. Changchun: Jilin University, 2016: 58–62.
- [41] 程桂亮, 姚奉洪, 杨开玉, 等. 耐热陶瓷的研究[J]. *中国陶瓷*, 1988(1): 22–28.
- Cheng G L, Yao F H, Yang K Y, et al. A study on temperware[J]. *China Ceramics*, 1988(1): 22–28.
- [42] Wang M, Zhu T Q, Ding X, et al. Composition comparison of Zhejiang Longquan celadon and its imitation in Dapu Kiln of Guangdong in the Ming Dynasty of China (1368—1644 CE) by LA-ICP-MS[J]. *Ceramic International*, 2018, 44(2): 1785–1796.